Available online at www.sciencedirect.com
ScienceDirect
Infrared Physics & Technology 50 (2007) 95–99
INFRARED PHYSICS & TECHNOLOGY
www.elsevier.com/locate/infrared

Autocorrelation measurements of free-electron laser radiation using a two-photon QWIP

H. Schneider [a,*], O. Drachenko [a], S. Winnerl [a], M. Helm [a], T. Maier [b], M. Walther [b]

[a] Institute of Ion-Beam Physics and Materials Research, Forschungszentrum Dresden Rossendorf, P.O. Box 510119, 01314 Dresden, Germany
[b] Fraunhofer-Institute for Applied Solid State Physics, Tullastrasse 72, D-79108 Freiburg, Germany

Available online 22 November 2006

Abstract

The two-photon QWIP comprises three equidistant subbands, namely two bound states localized in the quantum well and an extended state in the continuum. This device is very promising for quadratic autocorrelation measurements of pulsed mid-infrared lasers due to its resonantly enhanced optical nonlinearity and sub-ps time resolution. We report on interferometric autocorrelation measurements of ps optical pulses from a free-electron laser (FEL). The intense FEL radiation further allows us to study the saturation properties of two-photon QWIPs at liquid nitrogen temperature and their detection properties at 300 K. The device is well suited for standard diagnostics of the FEL pulse shape via interferometric autocorrelation.

1. Introduction

Quantum well infrared photodetectors (QWIPs) have emerged as a mature technology for thermal imagers [1]. Besides thermography, the high electrical bandwidth of QWIPs provides interesting opportunities in new applications including heterodyne detection [2] and optical pulse monitoring [3]. Intersubband transitions in quantum wells have also been exploited for second harmonic generation of mid-infrared radiation, and a huge coefficient, more than three orders of magnitude larger than for the host material GaAs, has been observed [4]. Nonlinear optical effects also enable quadratic detection through two-photon absorption. In this way, superior time resolution in the subpicosecond regime is readily achieved since the nonlinear process is not influenced by any parasitic time constants related to the device capacitance or resistivity.

While initial studies [5] employed two-photon absorption with a virtual intermediate state, much higher nonlinearities (more than six orders of magnitude higher than in bulk GaAs) have been reached in detectors comprising real intermediate states [6,7]. These two-photon QWIPs exploit *n*-type quantum wells with three equidistant levels, namely two bound subbands and one continuum resonance. In contrast to the (linear) QWIP, where one photon is sufficient to eliminate an electron from the quantum well (Fig. 1a), two infrared photons are then necessary for emission of an electron, as indicated in Fig. 1b. For this reason, the resulting photocurrent depends quadratically on the incident power.

We report here on interferometric autocorrelation measurements of mid-infrared laser pulses from the free-electron laser (FEL) facility FELBE at the Forschungszentrum Dresden Rossendorf [8]. Our results indicate that two-photon QWIPs are suitable for rapid-scan monitoring of the FEL pulse width. The observed autocorrelation signals show pronounced saturation effects under intense illumination. A detailed study of the intensity dependence indicates that the observed saturation behavior is associated with internal space charges, rather than absorption saturation or capacitive discharging. Finally, we also investigate the detection properties of two-photon QWIPs at room temperature.

* Corresponding author. Tel.: +49 351 260 2880; fax: +49 351 260 12880.
E-mail address: h.schneider@fzd.de (H. Schneider).

1350-4495/$ - see front matter © 2006 Elsevier B.V. All rights reserved.
doi:10.1016/j.infrared.2006.10.028

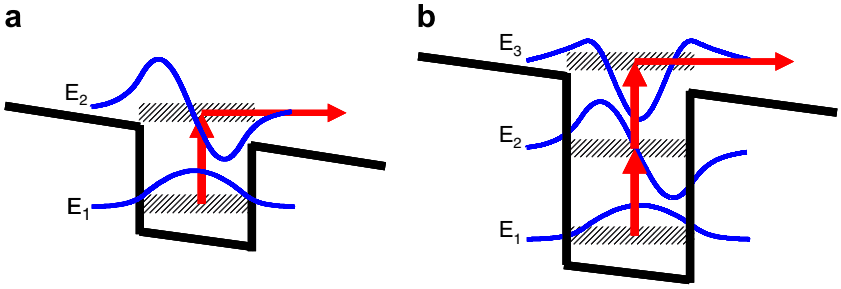

Fig. 1. Band diagram, wave functions, and operation principle of (a) linear and (b) two-photon QWIPs.

2. Experimental

The two-photon QWIP structures were grown by molecular beam epitaxy on semi-insulating GaAs substrates. Their active region contains 20 Si-doped quantum wells (4×10^{11} cm^{-2} electrons per well). The wafers were processed into mesa detectors of 120×120 μm^2 and 240×240 μm^2 in area. The radiation is coupled into the structure via 45°-facets. Sample X1649 comprises 7.6 nm wide GaAs quantum wells and 47 nm $Al_{0.33}Ga_{0.67}As$ barriers, which results in a peak detection wavelength of 10.4 μm. For sample X1654, we use 6.8 nm $In_{0.10}Ga_{0.90}As$ wells and 47 nm $Al_{0.38}Ga_{0.62}As$ barriers, with an observed peak wavelength of 8 μm. Further parameters are given in Ref. [6]. We have previously [6,7] demonstrated experimentally that the three relevant subbands of these two-photon QWIPs are energetically equidistant. Moreover, sub-ps population-relaxation (~0.5 ps) and dephasing (~0.1 ps) times have been demonstrated [6]. These time constants make these devices well suited for monitoring pulses in the ps regime.

For our autocorrelation measurements we employed a Michelson interferometer setup comprising a shaker (APE scan delay) with a scan frequency of typically 20 Hz on one arm, and a delay stage on the other arm (see Fig. 2). The photocurrent signal was recorded using a current preamplifier and a digital oscilloscope.

3. Interferometric autocorrelation

A typical interferometric autocorrelation trace is shown in Fig. 3. For quadratic detection, a ratio between the measured photocurrent for zero time delay and for temporally separated pulses in the case of interferometric autocorrela-

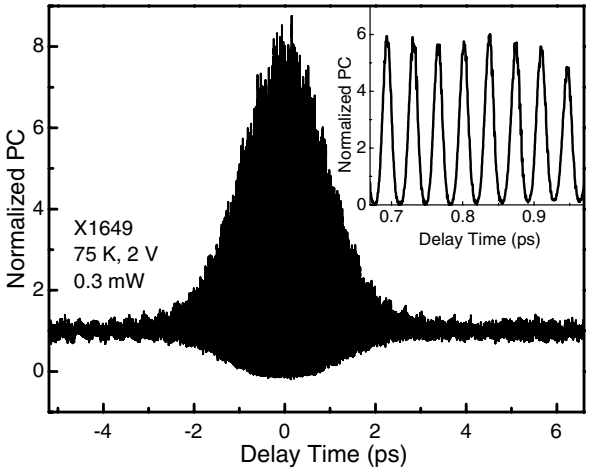

Fig. 3. Interferometric autocorrelation of FEL radiation using two-photon QWIP #X1649 at 0.3 mW incident power (about 1.3 kW/cm^2). Inset: Autocorrelation fringes vs. delay time in an expanded scale.

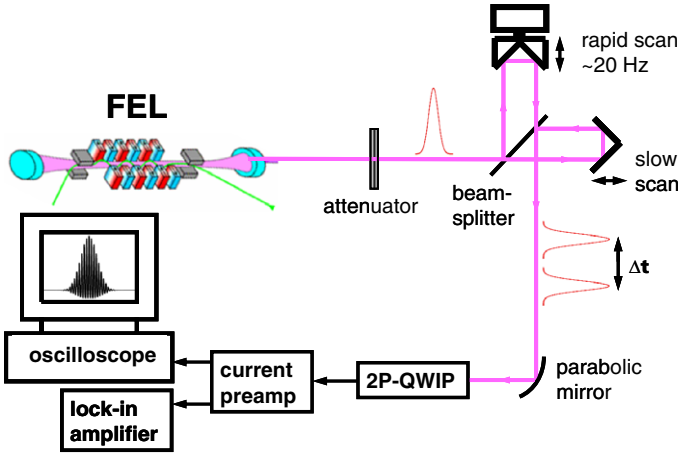

Fig. 2. Experimental setup for FEL autocorrelation measurements.

tion amounts to 8:1 [7]. The envelope of the measured interferometric autocorrelation reproduces this value to a good precision; the slightly higher value is attributed to some high-frequency noise during the measurement. Since the autocorrelation trace comprises over 100 fringes which are not resolved in Fig. 3, the inset shows a part of the autocorrelation trace in a magnified timescale. The asymmetric shape of the fringes constitutes an additional signature for the quadratic detection properties of the device. In fact, the fringes become perfectly sinusoidal if the square root of the signal is plotted (not shown) [9]. As the complete autocorrelation trace has been recorded in a single rapid scan (within about 25 ms) without any signal averaging, our approach is suitable for real-time monitoring of the FEL pulse properties. From Fig. 3, we deduce an autocorrelation width of 2.3 ps, which corresponds to a pulse duration of ~1.6 ps full-width at half maximum, giving rise to a FEL duty cycle of 2×10^{-5}.

4. Photocurrent saturation

Since the precise shape of the autocorrelation trace is crucial for its interpretation, it is important to investigate and to understand photocurrent saturation in these devices. In the case of linear QWIPs, it is well known [10,11] that screening of the electric field can induce photocurrent nonlinearities already at low excitation power. To investigate the intensity dependence of the two-photon QWIP signal, Fig. 4 shows the photocurrent as a function of the total average FEL power as measured by our external power meter. As can be seen from Fig. 4, the power dependence of the signal is truly quadratic at low power, whereas it saturates at a value between 15 and 20 μA. The two-photon responsivity S of two-photon QWIP #X1649 has been determined previously [6] and equals $S=4\times10^{-7}$ Acm^2/W^2 for continuous-wave radiation. For the duty cycle of 4×10^{-5} for two time-delayed FEL pulses, this value translates into $S=0.01$ Acm^2/W^2, which holds for the low-intensity regime far from saturation.

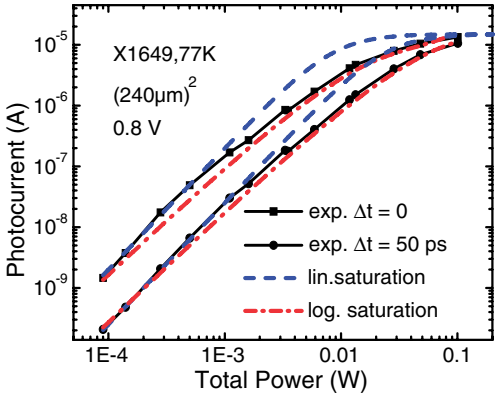

Fig. 4. Photocurrent of two-photon QWIP #X1649 and simulations for linear and logarithmic screening at zero delay and large delay, vs. total power.

Associating this value with the quadratic regime in Fig. 4, we found that only a few percent of the total power is actually focused into the active area of the two-photon QWIP device [9]. Using this calibration, photocurrent saturation is thus observed to occur at a threshold power of about 100 kW/cm^2 (corresponding to 20 mW total power in Fig. 4).

We now discuss different saturation mechanisms in order to understand better the observed saturation behavior. Absorption saturation is a first possible candidate for the observed saturation phenomenon. For linear QWIPs, Duboz et al. [12] have previously studied photocurrent saturation and found saturation effects only at very high power density (several MW/cm^2) where absorption saturation is expected to occur [1,12]. In our present study, we observe photocurrent saturation already at 100 kW/cm^2, such that absorption saturation can be excluded as a possible cause.

Lower saturation thresholds can occur due to field screening. To obtain a simple initial estimate, we consider the geometric capacitance of our samples, which amounts to 10 nF/cm^2 for a 1.1 μm wide active region (or to 5.8 pF for a 240×240 μm^2 device). Complete discharging of such a capacitor for, say, 1 V bias gives rise to a charge density of 6×10^{10} electrons/cm^2. This value is more than two orders of magnitude below the 8×10^{12} cm^{-2} electrons inside the quantum wells, which further excludes absorption saturation from causing the observed saturation. This estimate again suggests a threshold of the order of 10^5 Wcm^{-2} for space charge saturation, which agrees nicely with our experimental findings.

Let us therefore assume that the electric field inside the QWIP is screened by discharging the (geometric) capacitance of the device. Without screening, the photocurrent signal is given by $I=RP+SP^2$, with the linear and quadratic responsivities R and S, respectively. Taking the photoconductive gain g proportional to the electric field, linear field screening gives rise to the relation $g=(1-I/I_{\mathrm{Sat}})g_0$, with the low-intensity gain g_0 and the saturation current I_{Sat}. This results in the equation $I=(1-I/I_{\mathrm{Sat}})(RP+SP^2)$, which yields

$$I=\frac{I_{\mathrm{Sat}}(RP+SP^2)}{I_{\mathrm{Sat}}+(RP+SP^2)}. \tag{1}$$

Fig. 4 also incorporates the prediction of this linear saturation model (with $R=0$ for $T=77$ K). Obviously, the behavior at intermediate power density is not well described. Moreover, the observed saturation current is below 20 μA, whereas complete discharging of a 240×240 μm^2 device at 1 V bias and 13 MHz repetition rate would yield a significantly higher saturation current of 75 μA. We thus conclude that capacitive discharging is not yet appropriate for explaining the observed behavior, even though accurate saturation levels are predicted.

An alternative approach for space charge saturation is based on the low-power photocurrent nonlinearity [10,11]

known from linear QWIPs. In the stationary case, this nonlinearity is caused since the "first" barrier at the emitter side of the QWIP only bears a thermal current while the remaining barriers also carry a photoexcited current. The electric field thus has to be higher at the emitter barrier than in the rest of the active region in order to maintain the total current constant. To a good approximation, the thermal current depends exponentially on the electric field F (i.e., $I \sim \exp(\alpha F)$ with a prefactor α) if the voltage drop per QWIP period exceeds the thermal energy $k_B T$. Assuming again that the photocurrent is proportional to F, the above approximations lead to the relation $I = (\ln I_{Sat} - \ln I)(\tilde{R}P + \tilde{S}P^2)$ in the case of a two-photon QWIP with N quantum wells and $N+1$ barriers, with $\tilde{R} = R/N\alpha F$ and $\tilde{S} = S/N\alpha F$. This relation has the solution

$$I = (\tilde{R}P + \tilde{S}P^2) W\left(\frac{I_{Sat}}{\tilde{R}P + \tilde{S}P^2}\right), \tag{2}$$

where W is Lambert's W-function [13]. In the following, the model behind Eq. (2) will be referred to as logarithmic screening.

Applying this model to the experimental results of Fig. 4, logarithmic screening yields reasonably good agreement with the observed power dependence. However, there is still some deviation from the observed quadratic behavior at low intensity, as the W-function behaves like the logarithm for very large arguments. This deviation is presumably related with the assumption that the field is constant except for the emitter barrier, which is only valid in the stationary case. For weak excitation by short laser pulses, the space charge should be distributed over all quantum wells, which will presumably lead to some modification in the intensity dependence, but with similar functional behavior.

5. Autocorrelation in the presence of saturation

The influence of photocurrent saturation on autocorrelation measurements becomes most prominent when plotting the ratio between the maximum signal at zero time delay and the current I_{Inf} observed for time-separated pulses. Fig. 5 shows this ratio as a function of I_{Inf}, together with the predictions of the two screening models. As expected, the ratio goes to unity upon approaching saturation. A ratio of 8 was difficult to achieve experimentally even at low intensities, presumably owing to the logarithmic-like contribution predicted by Eq. (2). Applying Eqs. (1) and (2), we find in the case of linear screening

$$\text{ratio} = \frac{4SI_{Sat}^2}{SI_{Sat}(I_{Sat} + 7I_{Inf}) + 6R(Rx - y)} \frac{2y - Rx}{y + Rx}, \tag{3}$$

where $x = I_{Sat} - I_{Inf}$ and $y = \sqrt{x(R^2 x + 2SI_{Sat}I_{Inf})}$. For logarithmic screening, we define $u = \ln(I_{Sat}/I_{Inf})$, $v = \sqrt{u(u\tilde{R}^2 + 2\tilde{S}I_{Inf})}$ and obtain

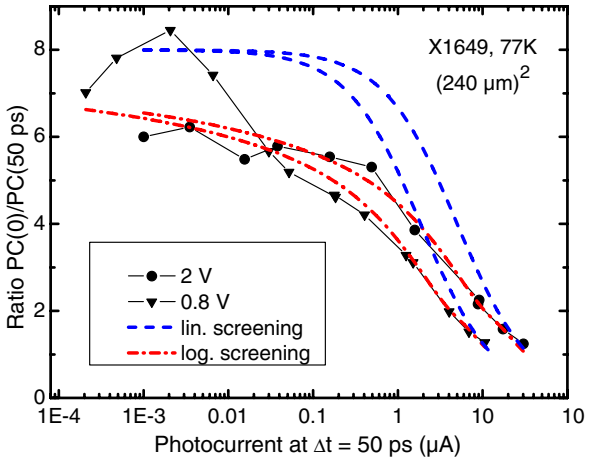

Fig. 5. Photocurrent ratio of two-photon QWIP #X1649 vs. photocurrent at $\Delta t = 50$ ps (77 K, 0.8 V and 2 V applied bias). Simulations using the linear and logarithmic screening models are also shown.

$$\text{ratio} = \frac{4}{u}\frac{2v - \tilde{R}u}{v + \tilde{R}u} W\left(\frac{\tilde{S}uI_{Sat}}{8\tilde{S}I_{Inf} + 6\tilde{R}(\tilde{R}u - v)}\right). \tag{4}$$

In the absence of linear photocurrent (i.e., $R = 0$), Eqs. (3) and (4) simplify to ratio $= 8I_{Sat}/(I_{Sat} + 7I_{Inf})$ and ratio $= 8W((I_{Sat}/8I_{Inf})\ln(I_{Sat}/I_{Inf}))/\ln(I_{Sat}/I_{Inf})$, respectively. Interestingly, the ratio then becomes independent of the quadratic prefactor S and thus only depends on the single parameter I_{Sat}. Taking this into account, the prediction of the logarithmic screening model is surprisingly good (see Fig. 5).

Linear screening yields strong deviations from the experimental behavior, though it seems to work better than logarithmic screening in the case of low intensity. As a consequence, it is experimentally possible to reach the desired ratio of 8:1 at low power. Since additional effects like dark current and thermal background current might be of some influence, this regime is not completely understood and needs further study.

6. Quadratic autocorrelation at room temperature?

As has been shown previously [6,7], thermal excitation into the intermediate subband induces a linear contribution to the signal. Fig. 6 shows the photocurrent induced by a CO_2 laser at 10.4 µm and 2.1 W/cm^2 vs. temperature. The fit curve is obtained from the equation

$$I = A + BT\exp\left(\frac{-E_A}{k_B T}\right), \tag{5}$$

where the coefficient A describes the two-photon photocurrent (which does not depend on temperature) and B the linear, thermally activated contribution. The fit yields an activation energy of $E_A = 105$ meV and points to a responsivity of 4 mA/W at room temperature for sample X1649 (about 1 mA/W at 300 K is expected for X1654 due to its

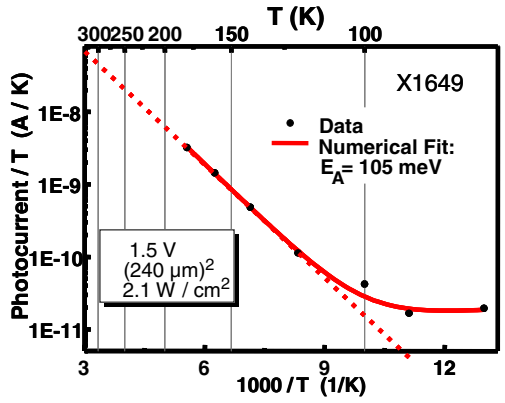

Fig. 6. Photocurrent of two-photon QWIP #1649 at 2.1 W/cm^2 vs. inverse temperature. The fit indicates an activation energy of 105 meV.

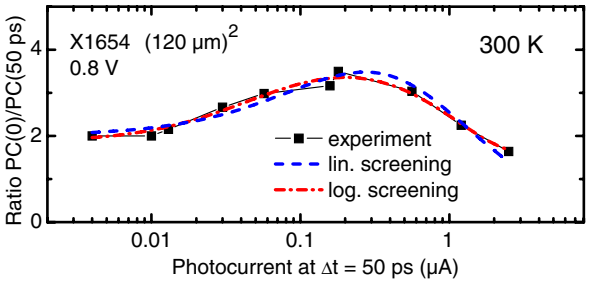

Fig. 7. Photocurrent ratio of two-photon QWIP #X1654 vs. photocurrent at $\Delta t = 50$ ps, (300 K, 0.8 V). Simulations using the linear and logarithmic screening models are also shown.

larger intersubband spacing). Consequently, the linear signal will dominate at low power.

Fig. 7 shows the photocurrent ratio vs. I_{Inf} for sample X1649 at room temperature. As expected, the ratio equals two at low power, which is clear evidence of linear behavior, and it approaches unity at high power due to saturation. In between, the maximum value is only 3.5, which indicates that the linear regime merges with the saturation regime. Fit curves according to Eqs. (3) and (4) are in nice agreement with the data, which is not unexpected owing to the number of fit parameters involved. Seemingly, Eq. (4) yields more accurate results than Eq. (3), which again favors logarithmic screening. Although the present devices do not appear suitable for quadratic autocorrelation measurements at room temperature, this goal should be achievable when using two-photon QWIPs designed for shorter detection wavelengths.

7. Conclusion

Two-photon QWIPs are useful devices for pulse characterization of free-electron laser radiation. Rapid-scan interferometric autocorrelation measurements allow for continuous monitoring of FEL pulse duration with high accuracy and enhancement factors up to the theoretically expected value of 8:1. The saturation behavior of the two-photon QWIP signal is limited by the generation of internal space charges, rather than absorption saturation or capacitive discharging. At room temperature, pure quadratic detection is inhibited by a linear, thermally activated signal arising from thermal population of the intermediate subband.

Acknowledgements

The authors are grateful to P. Michel and the whole ELBE team for their dedicated support. Part of this work has been supported by EuroMagNET under the EU contract RII3-CT-2004-506239 of the 6th Framework 'Structuring the European Research Area, Research Infrastructures Action'.

References

[1] H. Schneider, H.C. Liu, Quantum Well Infrared Photodetectors: Physics and Applications, Springer, Heidelberg, New York, 2006.
[2] P.D. Grant, R. Dudek, L. Wolfson, M. Buchanan, H.C. Liu, Electron. Lett. 41 (2005) 214.
[3] S. Steinkogler, H. Schneider, M. Walther, P. Koidl, Appl. Phys. Lett. 82 (2003) 3925.
[4] E. Rosencher, A. Fiore, B. Vinter, V. Berger, Ph. Bois, J. Nagle, Science 271 (1996) 168.
[5] A. Zavriyev, E. Dupont, P.B. Corkum, H.C. Liu, Z. Biglov, Opt. Lett. 20 (1995) 1885.
[6] H. Schneider, T. Maier, H.C. Liu, M. Walther, P. Koidl, Opt. Lett. 30 (2005) 287.
[7] T. Maier, H. Schneider, M. Walther, P. Koidl, H.C. Liu, Appl. Phys. Lett. 84 (2004) 5162.
[8] P. Michel, F. Gabriel, E. Grosse, P. Evtushenko, T. Dekorsy, M. Krenz, M. Helm, U. Lehnert, W. Seidel, R. Wünsch, D. Wohlfarth, and A. Wolf, in: Proceeding of the 26th International FEL Conference, Trieste, 2004. Available from: http://accelconf.web.cern.ch/AccelConf/f04/papers/MOAIS04/MOAIS04.pdfC.
[9] H. Schneider, O. Drachenko, S. Winnerl, M. Helm, M. Walther, Appl. Phys. Lett. 89 (2006) 133508.
[10] C. Mermelstein, H. Schneider, A. Sa'ar, C. Schönbein, M. Walther, G. Bihlmann, Appl. Phys. Lett. 71 (1997) 2011.
[11] M. Ershov, H.C. Liu, M. Buchanan, Z.R. Wasilewski, V. Ryzhii, Appl. Phys. Lett. 70 (1997) 414.
[12] J.Y. Duboz, E. Costard, J. Nagle, J.M. Berset, J.M. Ortega, J. Appl. Phys. 78 (1995) 1224.
[13] B. Hayes, Amer. Sci. 93 (2005) 104.